

# THE KPNO INTERNATIONAL SPECTROSCOPIC SURVEY. V. H $\alpha$ -SELECTED SURVEY LIST 3.

ANNA JANGREN, JOHN J. SALZER, VICKI L. SARAJEDINI<sup>1</sup>, CARYL GRONWALL<sup>2</sup>, JESSICA K. WERK<sup>3</sup>, LAURA CHOMIUK<sup>4</sup>  
 Astronomy Department, Wesleyan University, Middletown, CT 06459; anna@astro.wesleyan.edu, slaz@astro.wesleyan.edu

J. WARD MOODY

Department of Physics & Astronomy, Brigham Young University, Provo, UT 84602; jmoody@astro.byu.edu

AND

TODD A. BOROSON

National Optical Astronomy Obs., P.O. Box 26732, Tucson, AZ 85726; tyb@noao.edu

*Submitted 20 June 2005; Accepted 29 July 2005 – To appear in the 2005 December Astronomical Journal*

## ABSTRACT

The KPNO International Spectroscopic Survey (KISS) is an objective-prism survey designed to detect extragalactic emission-line objects. It combines many of the features of previous slitless spectroscopic surveys with the advantages of modern CCD detectors, and is the first purely digital objective-prism survey for emission-line galaxies (ELGs). Here we present the third list of ELG candidates selected from our red spectral data, which cover the wavelength range 6400 to 7200 Å. In most cases, the detected emission line is H $\alpha$ . The current survey list covers the region of the NOAO Deep Wide-Field Survey (NDWFS). This survey covers two fields; the first is  $3 \times 3$  degrees square and located at RA =  $14^h 30^m$ ,  $\delta = 34^\circ 30'$  (B1950), the second is  $2.3 \times 4.0$  degrees and centered at RA =  $2^h 7.5^m$ ,  $\delta = -4^\circ 44'$ . A total area of  $19.65 \text{ deg}^2$  is covered by the KISS data. A total of 261 candidate emission-line objects have been selected for inclusion in the survey list ( $13.3 \text{ per deg}^2$ ). We tabulate accurate coordinates and photometry for each source, as well as estimates of the redshift, emission-line flux and line equivalent width based on measurements of the digital objective-prism spectra. The properties of the KISS ELGs are examined using the available observational data. When combined with the wealth of multi-wavelength data already available for the NDWFS fields, the current list of KISS ELGs should provide a valuable tool for studying star-formation and nuclear activity in galaxies in the local universe.

*Subject headings:* galaxies: emission lines — galaxies: Seyfert — galaxies: starburst — surveys

## 1. INTRODUCTION

Surveys for galaxies containing active galactic nuclei (AGNs) or strong star-formation activity have been an important area of extragalactic astronomy for decades. Many fruitful surveys have been carried out with wide-field Schmidt telescopes used in conjunction with objective prisms. An overview of previous surveys is given in Salzer *et al.* (2000), along with a sampling of the types of applications that such surveys have for the study of the extragalactic universe.

We have been carrying out a modern objective-prism survey for the past several years. Called the KPNO International Spectroscopic Survey (KISS), it combines many of the advantages of older surveys with the use of state-of-the-art CCD detectors, providing superior depth and data quality. The digital nature of KISS has many advantages over the older photographic surveys of this type (e.g., Markarian 1967; Smith, Aguirre & Zemelman

1976; MacAlpine, Smith & Lewis 1977; Pesch & Sanduleak 1983; Wasilewski 1983; Markarian, Lipovetskii, & Stepanian 1983; Zamorano *et al.* 1994; Popescu *et al.* 1996; Surace & Comte 1998; Ugryumov *et al.* 1999). Besides the obvious factors of higher sensitivity and speed, we stress the importance of being able to measure the completeness limits and selection function of the survey directly from the data used to derive the catalogs of KISS emission-line galaxies (ELGs). This is not possible with photographic survey material, and makes KISS particularly useful for statistical studies of galaxian activity in the nearby universe.

The current survey lists cover the area of the sky included in the NOAO Deep Wide-Field Survey (NDWFS; Jannuzi & Dey 1999, Jannuzi *et al.* in preparation, Dey *et al.* in preparation). NDWFS is a deep optical and NIR imaging survey carried out in two well separated fields. All optical data were taken on the NOAO 4-m telescopes in the BRI bandpasses, while JHK imaging was carried out on the KPNO 2.1-m telescope. The fields were both covered to a uniform depth of  $B \approx 26.6$  (and correspondingly deep in the other five bands). We chose to observe these fields as part of KISS because of the expectation that they would become well observed at many wavelengths as various groups studied the properties of the NDWFS galaxies. While the primary science goals of the NDWFS focus on galaxies at redshifts well beyond

<sup>1</sup> Current address: Astronomy Department, University of Florida, Gainesville, FL, 32611; vicki@astro.ufl.edu.

<sup>2</sup> Current address: Department of Astronomy & Astrophysics, Pennsylvania State University, University Park, PA 16802; caryl@astro.psu.edu.

<sup>3</sup> Current address: Department of Astronomy, University of Michigan, Ann Arbor, MI 48109; jwerk@umich.edu

<sup>4</sup> Current address: Department of Astronomy, University of Wisconsin at Madison, 475 N. Charter St, Madison, WI 53706; chomiuk@astro.wisc.edu

the filter-imposed redshift limit of KISS ( $z \leq 0.095$ ), the volume covered by our survey is sufficiently large to provide a good-sized sample of star-forming galaxies and AGNs. Bolstered by the large amount of data becoming available for the galaxies in the NDWFS area at radio, FIR, NIR, UV, X-ray, and optical wavelengths, the KISS ELGs should allow for a number of detailed statistical studies of activity in galaxies in the local universe. While the KISS data are completely independent of the NDWFS data, they can be used to complement and extend the usefulness of the latter.

This is the fifth paper in the KISS series. The first presents a complete description of the survey method, including a discussion of the survey data and its associated uncertainties (Salzer *et al.* 2000; hereafter Paper I). The first and second survey lists of H $\alpha$ -selected ELGs, informally referred to as the red survey, are given in Salzer *et al.* (2001; hereafter KR1) and Gronwall *et al.* (2004; hereafter KR2), while the first list of [O III]-selected galaxies (the blue survey) is found in Salzer *et al.* (2002; hereafter KB1). The current paper follows a format similar to KR1 and KR2; for the sake of brevity, the reader is referred to KR1, KR2, and Paper I for many details. The observational data and image processing are described in Section 2, while the new list of ELG candidates is presented in Section 3. The properties of the new list of H $\alpha$ -selected ELGs are described in Section 4, while our results are summarized in Section 5.

## 2. OBSERVATIONS & REDUCTIONS

All survey data were acquired using the 0.61-meter Burrell Schmidt telescope<sup>5</sup>. The detector used for all data reported here was a  $2048 \times 4096$  pixel SITe CCD. The CCD is identical to the one used for the KR2 list, however this is not the same CCD that was used for KR1 or KB1, giving a different image scale and field-of-view. The CCD has  $15\text{-}\mu\text{m}$  pixels, yielding an image scale of  $1.43\text{ arcsec/pixel}$  at the Newtonian focus of the telescope. The overall field-of-view was  $50 \times 100\text{ arcmin}$ , and each image covered  $1.37\text{ square degrees}$ . The long dimension of the CCD was oriented north-south during our survey observations. The red survey spectral data were obtained with a  $4^\circ$  prism, which provided a reciprocal dispersion of  $17\text{ \AA/pixel}$  at H $\alpha$ . The spectral data were obtained through a special filter designed for the survey, which covered the spectral range  $6400 - 7200\text{ \AA}$  (see Figure 1 of Paper I for the filter transmission curve).

The two NDWFS fields each cover an area of  $9\text{ sq. deg.}$ . The spring (Boötes) field is centered at  $\text{RA} = 14^{\text{h}} 30^{\text{m}}$ ,  $\text{Dec} = 34^\circ 30'$  (B1950). It consists of a  $3 \times 3\text{ degree}$  square field. The fall (Cetus) field is a  $2.3 \times 4.0\text{ degree}$  area centered at  $\text{RA} = 2^{\text{h}} 7.5^{\text{m}}$ ,  $\text{Dec} = -4^\circ 44'$  (B1950). The layout of the Boötes field allowed us to cover the NDWFS area with two rows of KISS fields, with four fields per row. There is essentially zero overlap in declination between the two rows of fields. In addition, due to larger than normal pointing offsets between the direct and spectral fields (see below), there are modest gaps between some of the fields within a given row. The net result is that the KISS data for the Boötes field only cover  $8.08\text{ sq. deg.}$ , rather than the full  $9\text{ sq. deg.}$  For the Cetus fields,

we again utilized two rows of KISS fields. However, in this case there is substantial overlap between the upper and lower rows, due to the fact that the declination extent of this NDWFS region is smaller. Furthermore, we needed 6 KISS fields per row to cover the full  $4.0\text{ degrees}$  of RA. Despite the declination overlap, the Cetus KISS fields cover a total area of  $12.57\text{ sq. deg.}$ , substantially larger than the area of the NDWFS fields. The total area covered by the KISS observations is  $19.65\text{ sq. deg.}$

As with our previous survey strips, we obtained images of each survey field both with and without the objective prism on the telescope. The images taken without the prism (referred to as direct images) were obtained through standard B and V filters. The direct images were photometrically calibrated, and provide accurate astrometry and photometry for all sources in the survey fields. We used uniform exposure times for all survey fields:  $4 \times 720\text{ s}$  for the objective-prism (spectral) data, and  $2 \times 300\text{ s}$  for V and  $1 \times 600\text{ s}$  in B for the direct images. The telescope was dithered by a small amount ( $\sim 10\text{ arcsec}$ ) between exposures.

Table 1 lists the observing runs during which the current set of survey fields were observed. The first column gives the UT dates of the run, while the second column indicates the number of nights on which observations were obtained. At least some data were obtained on 12 of 14 scheduled nights (86%). The last two columns indicate the number of direct and spectral images, respectively, obtained during each run. It was common practice to observe in both direct and spectral modes during parts of each run, although it was not always the case that the direct and spectral images of a given field were obtained during the same run.

All data reduction took place using the Image Reduction and Analysis Facility (IRAF<sup>6</sup>) software. A special package of IRAF-based routines that were written by members of the KISS team was used for most of the data analysis. Full details of the observing procedures and data reduction methods are given in Paper I and KR1.

## 3. LIST 3 OF THE KPNO INTERNATIONAL SPECTROSCOPIC SURVEY

### 3.1. Selection Criteria

The selection of the third red (H $\alpha$ ) list of ELG candidates was carried out in precisely the same fashion as the first and second red lists (KR1 and KR2). Full details are presented in Paper I and KR1. To briefly summarize, we use our automated KISS software to evaluate the extracted objective-prism spectrum of each object located within a survey field. All objects with spectral features that rise more than five times the local noise above the continuum level are flagged as potential ELGs. This  $5\sigma$  threshold is the primary selection criterion of the survey, and was arrived at after substantial testing during the early phases of the KISS project. Following the initial automated selection, all candidates are visually examined, and spurious sources are removed from the sample. Finally, the objective-prism images are scanned visually

<sup>5</sup> Observations made with the Burrell Schmidt telescope of the Warner and Swasey Observatory, Case Western Reserve University.

<sup>6</sup> IRAF is distributed by the National Optical Astronomy Observatory, which is operated by the Association of Universities for Research in Astronomy, Inc., (AURA) under cooperative agreement with the National Science Foundation.

for sources that might have been missed by the software. These tend to be objects where the emission line is redshifted to the red end of the objective-prism spectrum, so that the software cannot detect continuum on both sides of the line. The combination of our automated selection process and our careful visual checking helps to ensure a high degree of reliability that the KISS ELG candidates are real, and that the sample is largely complete for all objects with  $5\sigma$  emission lines.

As described in KR1, we also flag objects that have emission lines between  $4\sigma$  and  $5\sigma$  during our selection process. These  $4\sigma$  detections represent objects with somewhat weaker emission lines than the main KISS sample, but that are nonetheless valid ELG candidates. However, these objects do not constitute a statistically complete sample in the same sense as the main ( $> 5\sigma$ ) list. We report the  $4$ – $5\sigma$  sources in a secondary list of ELG candidates (see Appendix), which should be thought of as a supplement to the main KISS catalog. This list of “extra” (or KISSRx) objects likely includes a number of interesting sources.

### 3.2. The Survey

The list of ELG candidates selected in the third red survey is presented in Table 2. Because the survey data includes both spectral images and photometrically-calibrated direct images, we are able to include a great deal of useful information about each source, such as accurate photometry and astrometry and estimates of the redshift, emission-line flux and equivalent width. Only the first page of the table is printed here; the complete table is available in the electronic version of this paper.

The contents of the survey table are as follows. Column 1 gives a running number for each object in the survey with the designation KISSR *xxxx*, where KISSR stands for “KISS red” survey. This is to distinguish it from the blue KISS survey (KB1). The KR1 and KR2 survey lists included KISSR objects 1–2157, and here we present KISSR objects 2158–2418. Columns 2 and 3 give the object identification from the KISS database tables, where the first number indicates the survey field (F*xxxx*), and the second number is the identification number within the field table for that galaxy. This identifier is necessary for locating the KISS ELGs within the survey database tables. Columns 4 and 5 list the right ascension and declination of each object (J2000). The formal uncertainties in the coordinates are 0.25 arcsec in RA and 0.20 arcsec in declination. Column 6 gives the B magnitude, while column 7 lists the B–V color. For brighter objects, the magnitude estimates typically have uncertainties of 0.05 mag, increasing to  $\sim 0.10$  mag at  $B = 20$ . Paper I includes a complete discussion of the precision of both the astrometry and photometry of the KISS objects. An estimate of the redshift of each galaxy, based on its objective-prism spectrum, is given in column 8. This estimate assumes that the emission line seen in the objective-prism spectrum is H $\alpha$ . Follow-up spectra for  $>1600$  ELG candidates from the two red survey lists (KR1, KR2 and the current list) show that this assumption is correct in the vast majority of cases. Only four ELGs in the current list that possess follow-up spectra (3%) are high redshift objects where a different line (typically [O III] and/or H $\beta$ ) appears in the objective-prism spectrum. The formal uncertainty in the redshift esti-

mates is  $\sigma_z = 0.0028$  (see Section 4.1.3). Columns 9 and 10 list the emission-line flux (in units of  $10^{-16}$  erg/s/cm $^2$ ) and equivalent width (in Å) measured from the objective-prism spectra. The calibration of the fluxes is discussed in section 4.1.2. These quantities should be taken as being representative estimates only. A simple estimate of the reliability of each source, the quality flag (QFLAG), is given in column 11. This quantity, assigned during the line measurement step of the data processing, is given the value of 1 for high quality sources, 2 for lower quality but still reliable objects, and 3 for somewhat less reliable sources. Column 12 gives alternate identifications for KISS ELGs which have been cataloged previously. This is not an exhaustive cross-referencing, but focuses on previous objective-prism surveys which overlap part or all of the current survey area: Markarian (1967) and Case (Pesch & Sanduleak 1983). The Markarian survey overlaps both the Boötes and Cetus fields, while the Case survey only overlaps the Boötes field. Also included are objects in common with the *Uppsala General Catalogue of Galaxies* (UGC, Nilson 1973).

A total of 261 ELG candidates are included in this third list of H $\alpha$ -selected KISS galaxies. The total area covered by the third red survey strip is  $19.65 \text{ deg}^2$ , meaning that there are 13.3 KISS ELGs per square degree. For the first, second, and third red lists combined, the surface density is  $16.4 \text{ galaxies deg}^{-2}$ , and if the lower significance KISSRx objects are included the density is  $20.7 \text{ ELGs deg}^{-2}$ . This compares to the surface density of  $0.1 \text{ galaxies deg}^{-2}$  from the Markarian (1967) survey, and  $0.56 \text{ galaxies per deg}^2$  from the H $\alpha$ -selected UCM survey (Zamorano *et al.* 1994); the present survey is much deeper despite the redshift limit inherent in our detection method. It is interesting to note that the fraction of  $4\sigma$  –  $5\sigma$  KISSRx ELG candidates is substantially higher for the sample presented here than for the first and second red survey areas. As discussed below, we believe that this difference is caused by the somewhat different noise characteristics of the CCD used for the current survey. For example, ELGs that would have been  $5.0\sigma$  objects when observed with the previous CCD might be detected as  $4.8\sigma$  sources in the current data. The net effect would be to lower the number of objects in the main survey list and to shift some of them into the KISSRx list. If both the lower-significance KISSRx objects and the *bona fide* KISSR objects are combined, the surface density of ELG candidates is essentially constant for all three red survey lists.

Of the 261 objects cataloged, 167 were assigned quality values of QFLAG = 1 (64%), 74 have QFLAG = 2 (28%), and 20 have QFLAG = 3 (8%). Based on our follow-up spectra to date, 99% (87 of 88) of the sources with QFLAG = 1 are *bona fide* emission-line galaxies, compared to 83% (24 of 29) with QFLAG = 2 and 78% (7 of 9) with QFLAG = 3. Overall, 94% of the objects with follow-up spectra are *bona fide* ELGs. The properties of the KISS galaxy sample are described in the next section.

Figure 1 shows an example of the finder charts for the KISS ELGs. These are generated from the direct images obtained as part of the survey, and represent a composite of the B- and V-band images. Figure 2 displays the extracted spectra derived from the objective-prism im-

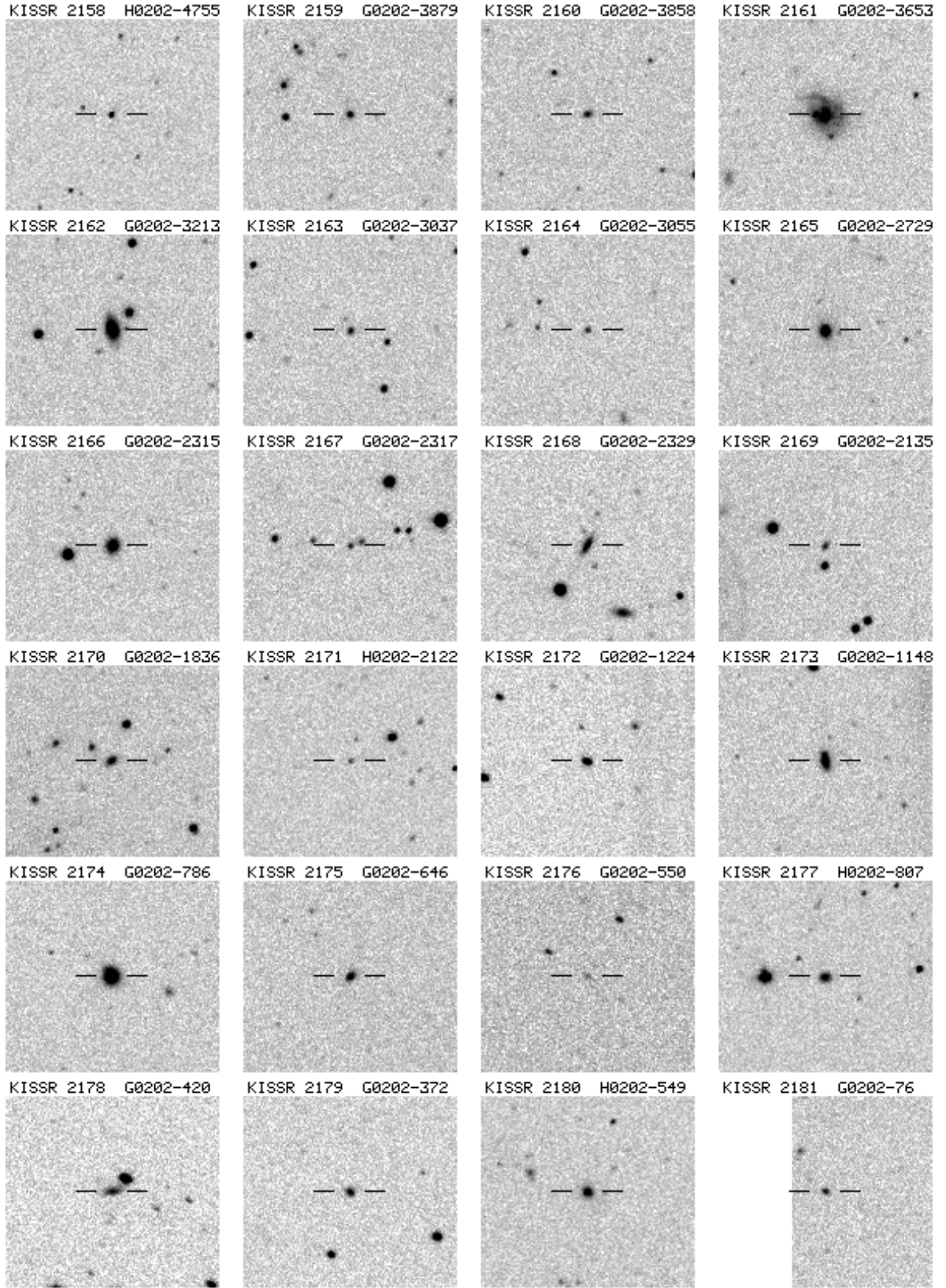


FIG. 1.— Example of finder charts for the KISS ELG candidates. Each image is  $3.2 \times 2.9$  arcmin, with N up, E left. These finders are created from a composite of the B- and V-band direct images obtained as part of the survey. In all cases the ELG candidate is located in the center of the image section displayed, and is indicated by the tick marks.

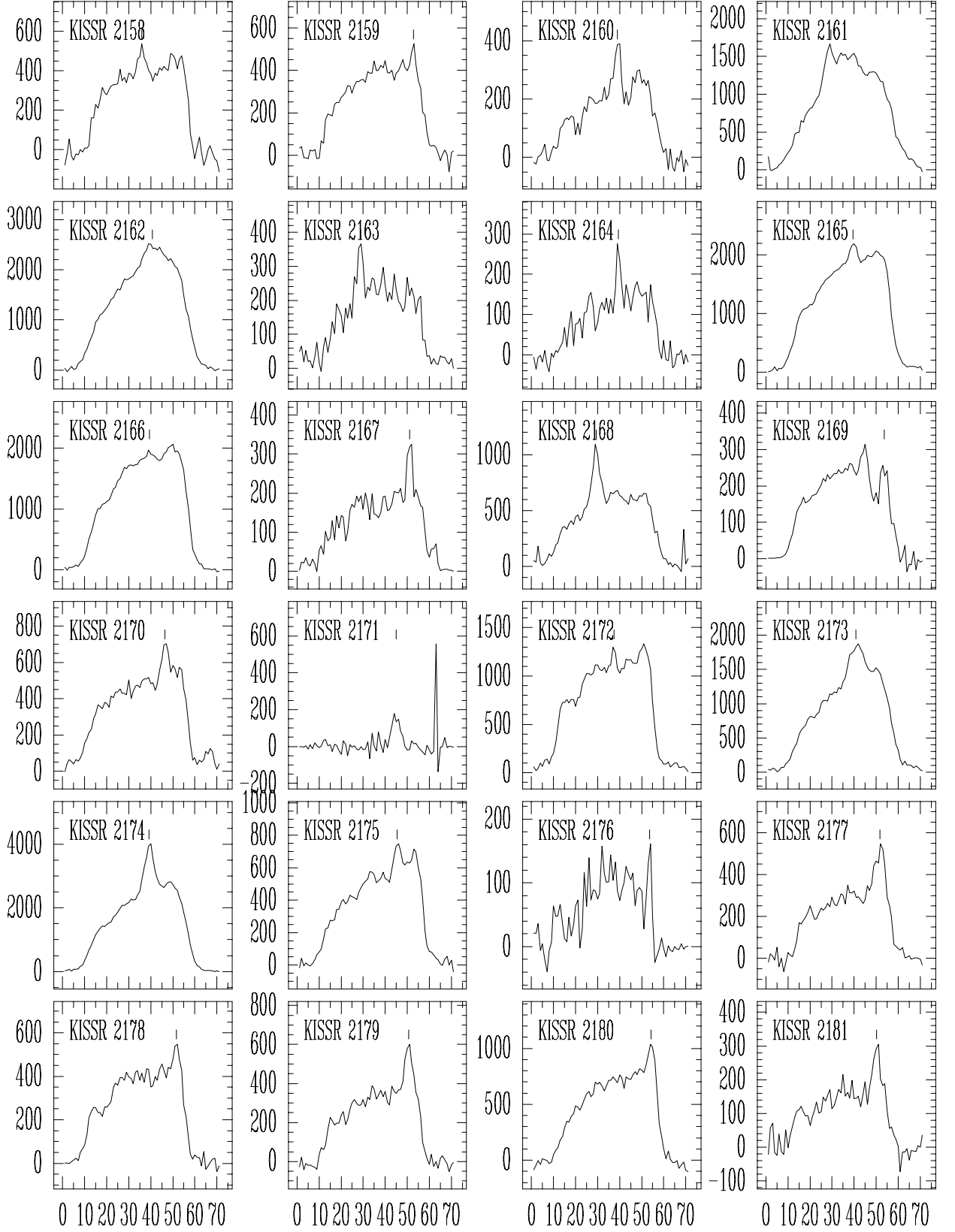


FIG. 2.— Plots of the objective-prism spectra for 24 KISS ELG candidates. The spectral information displayed represents the extracted spectra present in the KISS database tables. The location of the putative emission line is indicated.

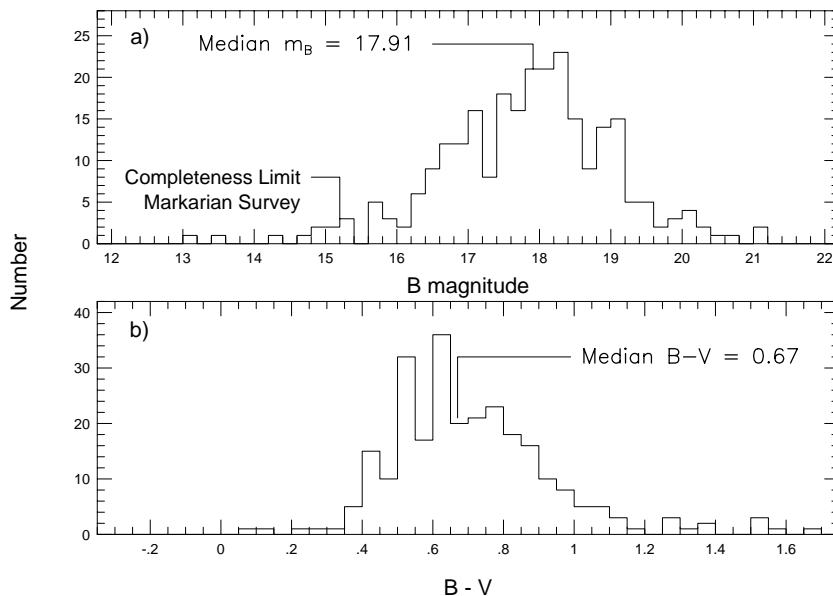


FIG. 3.— (a) Distribution of B-band apparent magnitudes for the 261 ELG candidates in the third  $H\alpha$ -selected KISS survey list. The median brightness in the KISS sample is  $B = 17.91$ , with 4% of the galaxies having  $B > 20$ . Also indicated, for comparison, is the completeness limit of the Markarian survey. (b) Histogram of the  $B-V$  colors for the 261 ELG candidates. The median color of 0.67 is indicated.

ages for the first 24 ELGs in Table 2. Finder charts and spectral plots for all 261 objects in the current survey list, along with finder charts for the KISSRx objects, are available in the electronic version of this paper.

A supplementary table containing an additional 158 ELG candidates with  $4\sigma$  to  $5\sigma$  emission lines is included in the appendix of this paper (Table 4). These additional galaxies do not constitute a statistically complete sample, and should therefore be used with caution. However, there are likely many interesting objects contained in this supplementary list. Hence, following the precedent established in KR1 and KR2, we list these objects in order to give a full accounting of the ELGs in the area surveyed.

#### 4. PROPERTIES OF THE KISS ELGS

Due to the manner in which the survey is carried out, a great deal of observational data are available for all of the KISS ELG candidates cataloged in the current paper. This includes accurate astrometry and B and V photometry for each source, as well as estimates of the redshift,  $H\alpha$  +  $[N\ II]$  line fluxes and equivalent widths. The combination of these data allow us to acquire a fairly complete picture of the make-up of the KISS sample. However, the quantities derived from the objective-prism spectra are inadequate for detailed analyses. First, the low resolution of the spectra limits the accuracy of the redshifts measured (see below). Further, the combination of low resolution and limited spectral coverage prevent us from using the survey data to ascertain the activity type of the ELGs (e.g., AGN vs. star-forming). Hence follow-up spectra obtained with a higher dispersion spectrograph are required for a complete understanding of the KISS

ELGs. Nonetheless, much can be gleaned about the survey constituents with the data currently available. We present an overview of the properties of our new sample of KISS ELGs below.

##### 4.1. Observed Properties

###### 4.1.1. Magnitude & Color Distributions

The B-band apparent magnitude distribution for the 261 KISS ELGs in the current survey list is shown in Figure 3a. The median apparent B magnitude is 17.91. This value is somewhat brighter than those of the KR1 and KR2 survey lists, which have median apparent magnitudes of  $B = 18.08$  and  $18.13$ , respectively. However, it is clear that KISS still probes substantially deeper than previous objective-prism surveys: The median apparent magnitude for the  $H\alpha$ -selected UCM survey (Pérez-González *et al.* 2000) is  $B \approx 16.1$ , and the  $[O\ III]$ -selected Michigan (UM) survey (Salzer *et al.* 1989) has a median apparent magnitude of  $B = 16.9$ . Indicated in the figure is the completeness limit of the Markarian survey,  $B = 15.2$  (Mazzarella & Balzano 1989).

The distribution of the  $B-V$  colors of the third red survey list is shown in Figure 3b. The median color is 0.67, which is identical to that of the first red survey list and very close to that of the KR2 survey list ( $B-V = 0.69$ ). This color is representative of an Sb galaxy (Roberts & Haynes 1994). The UCM survey shows a similar color distribution, and has a median color of  $B-r = 0.71$  (Pérez-González *et al.* 2000). In contrast, the  $[O\ III]$ -selected KB1 and UM surveys have color distributions that are significantly shifted to the blue, with median  $B-V$  colors of 0.50 and 0.55, respectively (KB1;

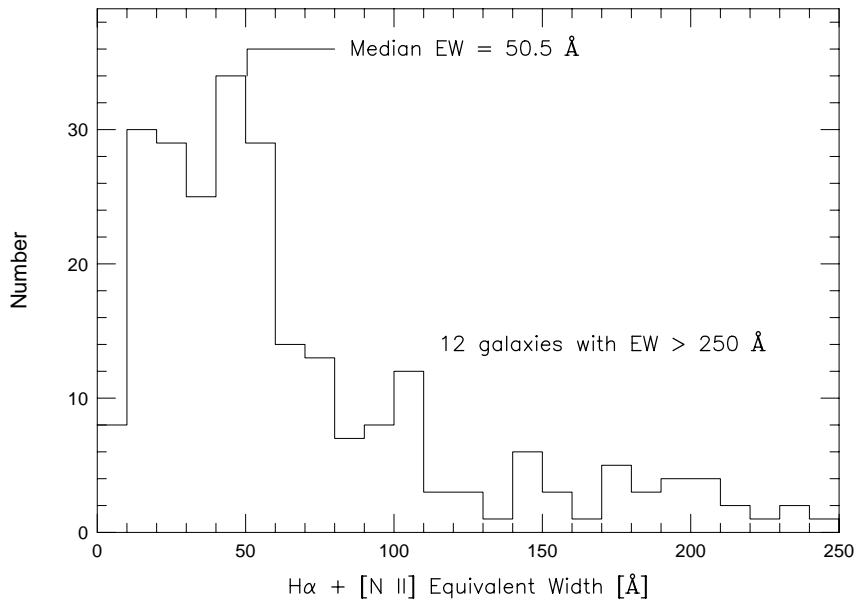


FIG. 4.— Distribution of measured  $H\alpha + [N II]$  equivalent widths for the KISS ELGs. The median value of  $50.5 \text{ \AA}$  is indicated. The measurements of equivalent widths from objective-prism spectra tend to show a large scatter when compared to equivalent widths from long-slit spectra, so these values should be taken only as estimates. The survey appears to detect most sources with  $EW(H\alpha + [N II]) > 30\text{--}40 \text{ \AA}$ .

Salzer *et al.* 1989). This is a selection effect caused by the use of different emission lines for detection in the different surveys. The  $H\alpha$ -selected samples include a broader spectrum of ELGs, including many more luminous star-forming galaxies and LINERS which tend to be dominated by older, redder stellar populations. In addition, they are able to detect galaxies with higher levels of intrinsic reddening. The  $[O III]$ -selected samples are dominated by lower luminosity, lower metallicity galaxies which are dominated by younger stellar populations and have lower levels of internal absorption and reddening. While the  $H\alpha$ -selected surveys tend to include both types of ELGs, they are dominated by the more luminous galaxies. In contrast, the blue-selected surveys tend to not select the redder galaxies at all.

#### 4.1.2. Line Strength Distributions and Survey Completeness

The distribution of equivalent widths (EWs) for the third red survey list is shown in Figure 4. We assume that the line we measure in the survey spectra is  $H\alpha$  blended with the  $[N II]\lambda\lambda 6584, 6548$  lines. Based on follow-up observations obtained to date, we know this assumption to be true for the vast majority of red survey objects. The three lines are blended at the resolution of the objective-prism spectra. The  $[S II]\lambda\lambda 6731, 6717$  doublet is well resolved from the blended  $H\alpha + [N II]$  lines, and is often seen in survey spectra from strong-lined objects. The EW distribution peaks in the  $40\text{--}50 \text{ \AA}$  bin, which indicates that KISS is fairly complete for objects with equivalent widths greater than  $\sim 50 \text{ \AA}$ . The median equivalent width of  $H\alpha + [N II]$  is  $50.5 \text{ \AA}$ , with the majority of

ELGs having equivalent widths of less than  $100 \text{ \AA}$ . This median EW is approximately 25% higher for this sample than for the two previous red survey lists. The noise level in the third red survey list data is slightly higher than for the first and second red survey list. We attribute this to the use of a different CCD for the newer sample, which had somewhat worse noise characteristics than the previous CCD. This shift in noise characteristics results in a selection of  $5\sigma$  ELG candidates that have relatively stronger lines. As we mention above the fraction of  $4\sigma\text{--}5\sigma$  objects is higher for the survey list presented here than for the two previous red survey lists, which is what we expect due to a higher noise level.

The calibration of the flux scale is a two-step process. The objective-prism spectra for each field are first corrected for throughput variations and atmospheric extinction. This places all line fluxes on the same *relative* flux scale. The fluxes are then calibrated on an absolute scale, using information obtained from the follow-up spectra. From a sample of 126 follow-up observations, we selected 49 objects that were classified as star-forming galaxies, had spectral quality  $Q = 1$  or 2, and had been observed with a long-slit spectrograph under photometric conditions. All spectra were obtained during the same observing run, and are of galaxies located in the Boötes field. Since the fluxes measured from the objective-prism spectra are a combination of the  $H\alpha$  and  $[N II]$  lines, we use the fluxes from our slit spectra for the sum of these three lines. Figure 5 shows a plot of the ratio of objective-prism flux (in counts) to spectroscopic flux *versus* the equivalent width measured from the follow-up spectra. The majority of the emission-line flux from a point source was in-

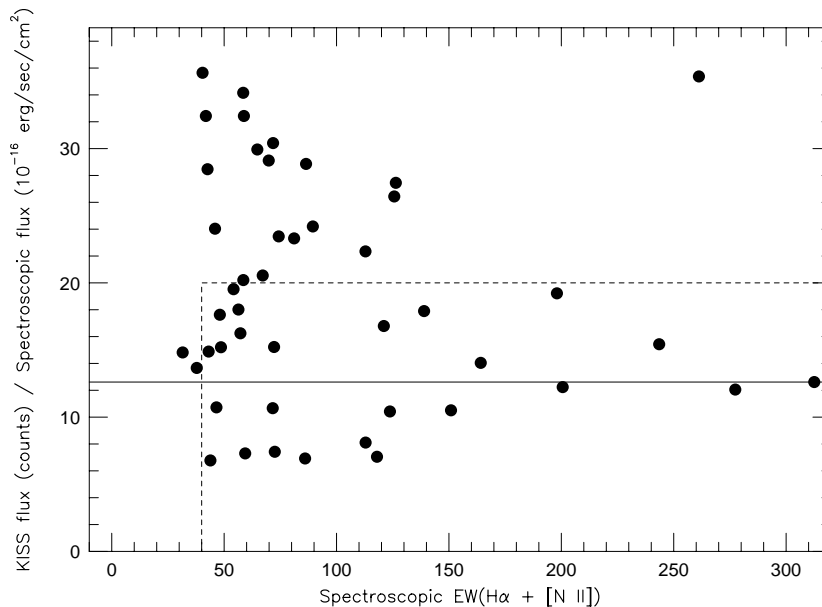


FIG. 5.— Plot of the ratio of objective-prism flux (in counts) to spectroscopic flux *versus*  $H\alpha + [N II]$  equivalent width measured from the follow-up spectra. The plotted data are all from the same observing run (KPNO 2.1-m, 2004). The solid line indicates the median ratio. The dashed lines show the criteria we applied to select the calibration sample. One galaxy with flux ratio  $> 40$  falls above the diagram, and another galaxy with  $EW > 320 \text{ \AA}$  lies off the diagram to the right.

cluded in the follow-up spectra, since the slit width used was  $2.0''$ . Some galaxies, however, have a larger angular extent and the emission lines originate in an extended region. Since our long-slit measurements do not include all the  $H\alpha$  emission from these sources, they tend to have large flux ratios. We restricted the calibration sample to those galaxies with an objective-prism-to-spectroscopic flux ratio of less than 20 and an equivalent width greater than  $40 \text{ \AA}$ , which left 25 galaxies. The emission regions of these galaxies are essentially point sources. The median flux ratio of the calibration sample is 12.61; the mean is 12.92 with a standard deviation of 4.19 and an error in the mean of 0.84. We adopted the reciprocal of the median value as our calibration value, or  $0.0793 \times 10^{-16} \text{ ergs/s/cm}^2$  per count.

The calibration value is applied to the measured objective-prism line fluxes to convert their instrumental fluxes (in counts) to calibrated fluxes (in  $\text{ergs/s/cm}^2$ ). In Figure 6 we show the distribution of observed  $H\alpha + [N II]$  line flux values for the 261 KISS ELGs. The median value is  $1.05 \times 10^{-14} \text{ ergs/s/cm}^2$ , which is  $\sim 30\%$  higher than the values found for the first two red survey lists, suggesting that the data used for the current survey is less sensitive than those used for the first and second red survey lists. As we mention above, this difference is likely due to the slightly higher noise level in the KR3 data. However, the median line flux of the third red survey list is substantially fainter than that of the UCM sample, which is  $2.9 \times 10^{-14} \text{ ergs/s/cm}^2$  (based on follow-up spectra of Gallego *et al.* 1996).

As mentioned earlier, one of the strengths of KISS is that the selection function and completeness limit can be

derived using the survey data directly, rather than relying on secondary information (e.g., line strengths measured from follow-up spectra). The calibrated objective-prism line fluxes are used to determine the completeness limit of the survey, following the procedure described in Gronwall *et al.* (2005, in preparation). Briefly, we convert the line fluxes into pseudo-magnitudes – the line magnitude  $m_L$ , and then apply a  $V/V_{max}$  analysis (e.g., Schmidt 1968, Huchra & Sargent 1973) to the complete sample of 261 galaxies. The results are presented in Table 3. Column (1) lists  $m_{comp}$ , the value of  $m_L$  for which  $\langle V/V_{max} \rangle$  is being computed. Column (2) lists the total number of ELGs brighter than that  $m_L$  level, while columns (3) and (4) give the numbers of objects in the volume-limited and flux-limited subsamples, respectively (see below). Note that some objects may start out in the flux-limited sample at brighter values of  $m_{comp}$ , then move into the volume-limited sample at fainter values of  $m_{comp}$ . Column (5) lists the mean  $V/V_{max}$  for the flux-limited subsample. Column (6) shows the number of galaxies that need to be added to the sample at each  $m_{comp}$  level to maintain  $\langle V/V_{max} \rangle = 0.5$ , and column (7) lists the cumulative number of galaxies added at all magnitudes brighter than the given magnitude level to maintain  $\langle V/V_{max} \rangle$ . Column (8) shows the percentage of objects that are in the flux-limited subsample, which decreases continuously as  $m_L$  becomes fainter. Column (9) lists the completeness percentage of the flux-limited subsample as a function of  $m_L$ . These latter two quantities are plotted in Figure 7.

The interpretation of the results of the  $V/V_{max}$  test follows exactly the discussion found in Gronwall *et al.*

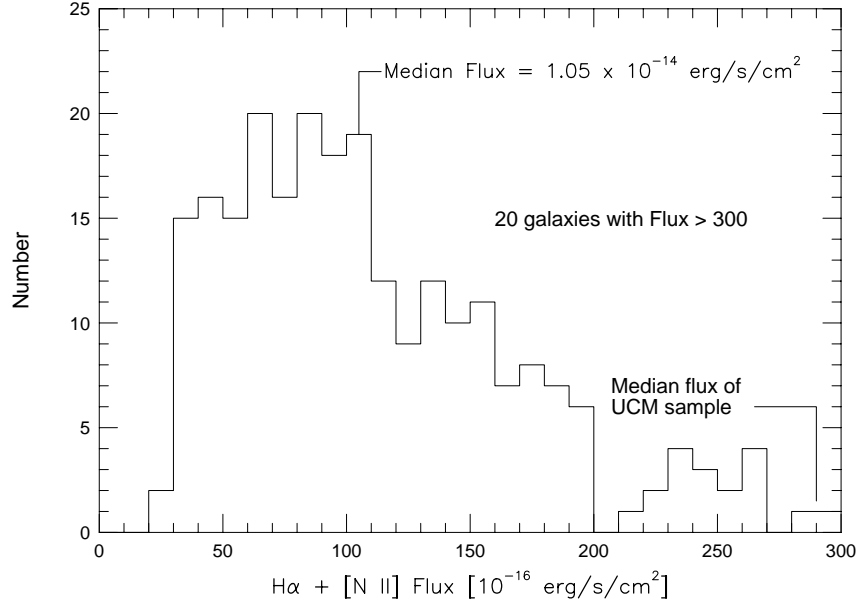


FIG. 6.— Distribution of  $H\alpha + [N II]$  line fluxes for the 261 KISS ELGs included in the current survey list. The median flux level of both the KISS and UCM samples is indicated.

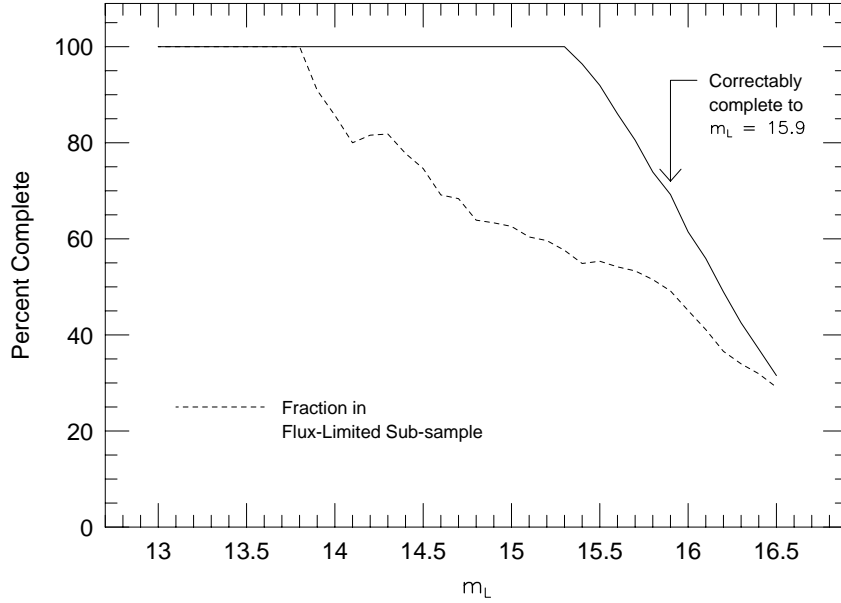


FIG. 7.— Plot of the completeness percentage as a function of  $m_L$  for the current sample (solid line). The catalog is 100% complete to  $m_L = 15.3$ , and is “correctly complete” to  $m_L = 15.9$ . The dashed line shows the fraction of the sample contained in the flux-limited sub-sample as a function of  $m_L$ . At the completeness limit, roughly half of the KISS ELGs are in the flux-limited portion of the sample.

(2005, in preparation) for the KR1 sample. Rather than repeating that discussion here, we will simply summarize the main results. It is important to realize that because of the redshift limit imposed by the survey fil-

ter, objects in the sample can be either line-flux-limited or volume-limited objects, depending on the strength of their  $H\alpha + [N II]$  emission and their redshift. Objects with sufficiently strong lines will have values of  $V_{max}$  that ex-

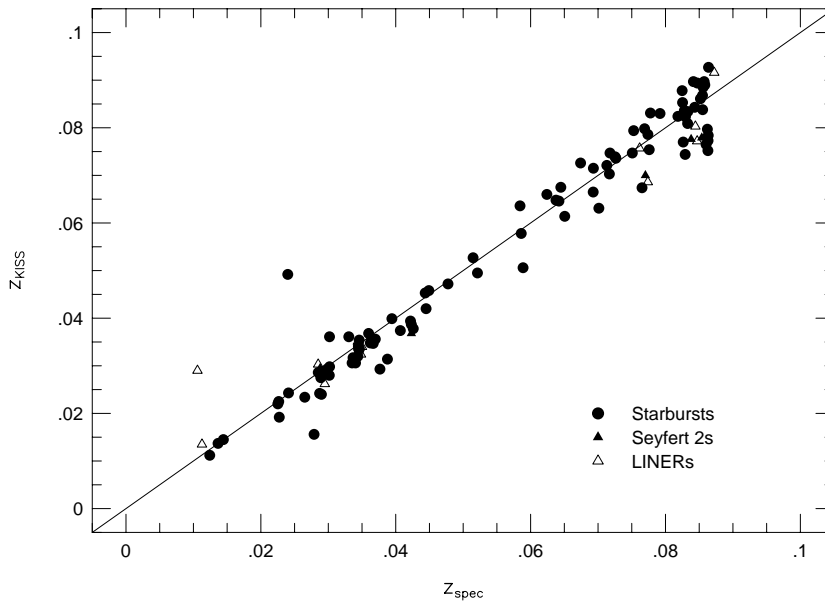


FIG. 8.— Comparison between objective-prism redshifts ( $z_{KISS}$ ) obtained from our survey data and slit-spectra redshifts ( $z_{spec}$ ) obtained from follow-up spectra. The solid line denotes  $z_{KISS} = z_{spec}$ . The objective-prism redshifts provide reasonable estimates of the true redshifts over the full range covered by the survey. The formal uncertainty in  $z_{KISS}$  is 0.0032 (950 km s<sup>-1</sup>).

ceed the effective volume of the survey set by the redshift limit. Such objects are volume limited. As the limiting line flux (parameterized by  $m_L$ ) decreases, a given object may actually switch from being in the flux-limited category to the volume-limited category. As seen in the table, for faint limiting line fluxes (fainter  $m_L$ ) the majority of the KISS ELGs are in the volume-limited subsample. This is illustrated by the dashed line in Figure 7. We see that the KISS sample is 100% complete to  $m_L = 15.3$ , which is very similar to the results for the KR1 and KR2 samples (Gronwall *et al.* 2004, 2005). This completeness limit includes 184 KISS ELGs, or 70.5% of the full sample. As is often done, one can construct a “correctably complete” sample by extending the line-flux limit down to even lower values. For example, at  $m_L = 15.9$ , the sample is still 69.2% complete, but now includes 91.2% of the sample.

#### 4.1.3. Redshift Comparison and Distributions

We also derive redshifts from the objective-prism spectra. For objects with follow-up observations, we can compare the survey redshifts to the redshifts derived from the long-slit spectra (Figure 8). In general the agreement between  $z_{KISS}$  (objective-prism redshift) and  $z_{spec}$  (follow-up redshift) is excellent. Only four objects deviate substantially from the equality line. Two of these are active galaxies at  $z > 0.35$  which are not shown in the diagram. They were detected due to their [O III] $\lambda$ 5007 and H $\beta$  lines, respectively. The remaining two objects are KISSR 2336 and KISSR 2320; two relatively large, well-resolved disk galaxies that both have emission regions which are offset from the center of the galaxy. Because the dispersion of the objective-prism spectra is in the

north-south direction, a spectrum of an object that has an emission region spatially offset north or south of the center will yield an incorrect estimate of the redshift of the emission line. Only a small minority of KISS objects are affected by this.

For the first red survey list (KR1) the survey redshifts above  $z_{KISS} = 0.07$  showed a systematic offset from the redshifts determined from follow-up spectroscopy. The reason for the offset is that as the H $\alpha$  + [N II] line in the objective-prism spectrum begins to shift out of the survey bandpass, only the lower-redshift portion of the line is detected. A correction was applied to the KR1 survey redshifts, as described in Paper I. The objects plotted in Figure 8 do not display this offset, and no correction was applied to the survey redshifts. The second red survey list (KR2) also did not show any systematic offset. The reason for the difference is probably the better pixel scale of the CCD used for the second and third red survey lists. When we calculate the RMS scatter of  $z_{KISS}$  about the equality line we use only objects with  $z_{spec} < 0.07$ , as was done for KR1. We exclude the four most deviant objects that we described in the previous paragraph. The resulting RMS scatter is 0.0032 (950 km/s), which is marginally higher than the value found for the first two red survey lists (0.0028, or 840 km/s).

The distribution of the objective-prism redshifts is shown in Figure 9. The Boötes and Cetus fields are shown in separate panels. The middle panel shows the redshift distribution for a comparison sample of galaxies from Zwicky *et al.* (1961 – 1968; hereafter CGCG). The redshifts for the 97 CGCG galaxies are taken from Falco *et al.* (1999). Since the surface density of the CGCG catalog is fairly low, we included objects located in a region

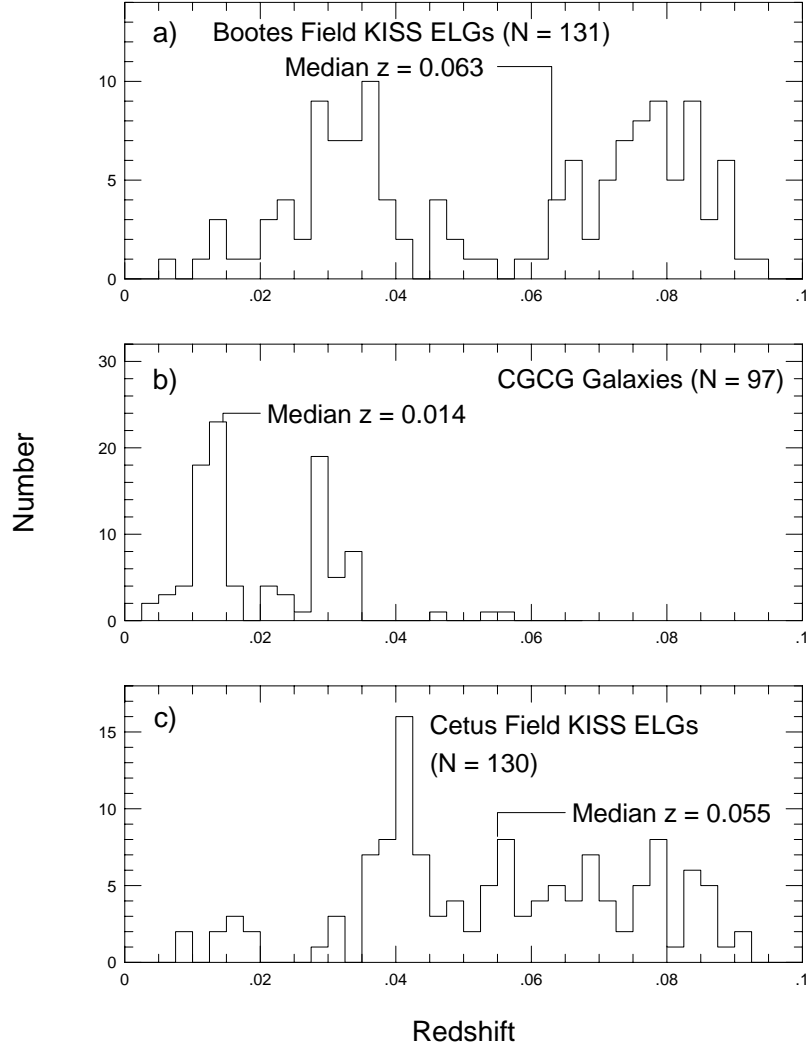


FIG. 9.— Histograms showing the distribution of redshift for the 261 H $\alpha$ -selected KISS ELGs in (a) the Boötes field and (c) the Cetus field. In (b) we show the distribution of 97 “normal” galaxies from the CGCG that are located in the area of the Boötes field. The median redshift is indicated in all plots. The deficit of ELGs between  $z = 0.04$  and  $0.06$  seen in (a) is due to the Boötes void.

of  $9 \times 9$  degrees, centered at the location of the Boötes field. The CGCG catalog does not extend far enough south to overlap the Cetus field, hence the comparison sample applies only to the upper (Boötes) redshift sample.

The Boötes void (Kirshner *et al.* 1981) is clearly visible between  $z = 0.04$  and  $z = 0.06$  in Figure 9a. Even though the NDWFS field is located far south of the nominal void center, the impact of the void is unmistakable in the redshift distribution. There is a significant density enhancement seen at redshifts between 0.0275 and 0.0375, just in front of the void. This is most likely associated with the Hercules supercluster. A modest peak in the redshift distribution of the CGCG sample is also seen in this redshift range. The latter becomes quite sparse beyond this redshift. The CGCG sample also shows a

strong peak at  $z = 0.0125$  which is less prominent in the KISS distribution. Of the 41 CGCG galaxies that constitute this peak, only four are found inside the Boötes field survey area. The galaxies in this peak appear to fall along a large-scale structure feature that falls mostly outside the NDWFS area. Beyond the Boötes void the KISS sample displays a fairly flat redshift distribution out to  $z \sim 0.085$ , after which it begins to drop off. The distribution drops to zero at  $z = 0.095$ , because KISS cannot detect galaxies via the H $\alpha$  line beyond this distance since it redshifts completely out of the survey filter at this point. The flat distribution and drop-off between 0.085 and 0.095 are characteristic of what is seen with the KR1 and KR2 samples as well.

The redshift distribution for the Cetus field (Figure 9c) is dominated by a low density region at low redshifts that

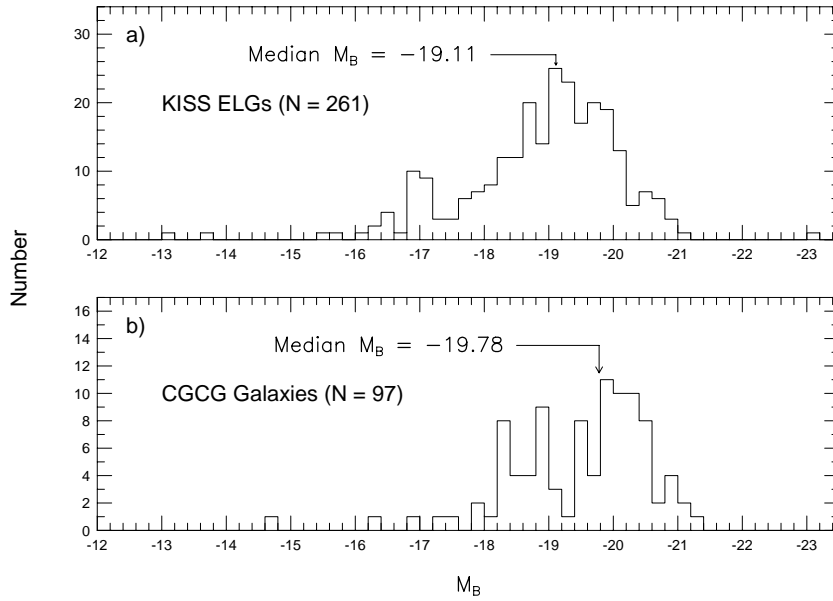


FIG. 10.— Histograms showing the distribution of blue absolute magnitude for (a) the  $H\alpha$ -selected KISS ELGs from the two survey fields and (b) the 97 “normal” galaxies from the CGCG that are located in the Boötes field area of the sky. The median luminosity of each sample is indicated. The KISS ELG sample is made up of predominantly intermediate- and lower-luminosity galaxies, making this line-selected sample particularly powerful for studying dwarf galaxies.

reaches out to  $z = 0.035$ . This is part of the large void that dominates the foreground in the south Galactic cap. There is no hint of the Pisces-Perseus supercluster at  $z \approx 0.020$ ; the Cetus field is far enough south to miss the supercluster. There is a strong density enhancement at  $z = 0.040$ . Beyond this point, the KISS redshift distribution is again fairly flat out to the point where the survey filter starts to exclude the  $H\alpha$  line. Note that the location of the Cetus field is such that only very sparse redshift information of the “normal” galaxies exists. Hence, we do not have a suitable comparison sample as we do with the Boötes field.

The median redshifts of the two NDWFS KISS samples are quite similar to the values found for KR1 (median  $z = 0.063$ ) and KR2 (median  $z = 0.061$ ).

#### 4.2. Luminosity Distributions

The availability of both an accurate apparent magnitude and a redshift estimate allows us to compute the absolute magnitude for each source. Using the values listed in Table 2 for the B magnitude and objective-prism redshift, we compute  $M_B$  for all ELG candidates in the current list.  $H_0 = 75$  km/s/Mpc is adopted, and a correction for Galactic absorption is applied using the values for  $A_B$  compiled by Schlegel *et al.* (1998). In both fields the Galactic absorption is small, with typical values of  $0.04 - 0.06$  mags in the Boötes field, and  $0.09 - 0.11$  mags in the Cetus region. An explicit assumption made is that the line seen in the objective-prism spectrum is in fact  $H\alpha$ . Previous observations of KR1 and KR2 ELGs suggest that for roughly 2.5% of the KISS ELG candidates the line seen in the objective-prism spectrum is some other line (usually [O III] $\lambda 5007$ ). Hence we might

expect 6-7 of the ELG candidates in Table 2 to fall in this category.

A histogram showing the distribution of  $M_B$  for the KISS ELGs in the current survey list is shown in Figure 10a. For comparison, in Figure 10b we plot the absolute magnitude distribution for the 97 CGCG galaxies used in the redshift distribution comparison in the previous subsection. Note that for this presentation we have combined the two portions of the KISS NDWFS sample into a single histogram. The median absolute magnitudes of the KISS and CGCG galaxies differ significantly: While the CGCG has a median  $M_B = -19.78$  (i.e., close to  $M^*$ ), the KISS ELGs have a median absolute magnitude fully 2/3rds of a magnitude fainter. This is consistent with our previous survey lists. That is, KISS is especially sensitive to intermediate and low luminosity galaxies when compared to a magnitude-limited sample like the CGCG.

Despite the fact that the current sample of KISS ELGs have systematically lower luminosities than the CGCG galaxies located in the same area of the sky, they are, on average, *higher* in luminosity than either of the previous two  $H\alpha$ -selected KISS lists. The median  $M_B$  values for KR1 and KR2 are  $-18.96$  and  $-18.64$ , respectively. The apparent reason for the differences between the three lists is the relative paucity of lower redshift galaxies in the current survey. As mentioned above, the Cetus and Boötes fields of the NDWFS exhibit very low numbers of galaxies at redshifts below 0.035 and 0.025, respectively. This is precisely where KISS is most sensitive to dwarf ELGs. To be sure, there are still plenty of low luminosity galaxies present in the current survey list. However, the fraction of the survey with  $M_B > -18$  is less than in

both KR1 and KR2.

At the high luminosity end, the KISS ELGs appear to be deficient in galaxies with luminosities above  $M^*$  ( $M_B < -20$ ). While the KISS ELGs cover the same absolute magnitude range as the magnitude-limited CGCG galaxies, the proportion of higher luminosity galaxies is much lower among the KISS galaxies. This most likely occurs for two reasons. First, the KISS sample is redshift limited at high luminosities, meaning that it does not probe arbitrarily large volumes of space for the highest luminosity objects as magnitude-limited samples do. Second, the detection of any galaxy by KISS requires that the emission line observed be bright enough to stand out against the stellar continuum of the galaxy in the objective-prism spectrum. That is, there must be a minimum contrast between the continuum and the line. This is effectively an equivalent width limit. For luminous galaxies, a larger star-forming event or a stronger level of AGN activity is needed for the emission lines to exceed this implicit equivalent width threshold. Since these intense activity levels are fairly rare, there are fewer detected ELGs among the higher luminosity host galaxies. The combination of these two effects means that there are fewer KISS ELGs at luminosities above  $M^*$ .

#### 4.3. Comparison with Previous Surveys

Table 2 lists cross-references for KISS ELGs which are also cataloged in previous photographic surveys for active and star-forming galaxies, and we note the UGC numbers for the objects that are listed in the *Uppsala General Catalogue of Galaxies* (Nilson, 1973). The first red survey area overlapped with four major active galaxy surveys: Markarian (1967), Case (Pesch & Sanduleak 1983), Wasilewski (1983), and UCM (Zamorano *et al.* 1994). The third red survey area, like KR2, overlaps with only the Markarian and Case surveys.

The Markarian survey overlaps both the Boötes and Cetus fields. There are, however, no Markarian galaxies in either field. This is not too surprising, since the surface density of Markarian galaxies is small (0.1 per sq. deg.). The Case survey overlaps only with the Boötes field, and there are 18 Case objects in this area. However, two of them lie just outside the area covered by the KISS objective-prism images. They are both included in the KISS direct images, but as we mention in §2, the spectral and direct images do not always cover the exact same area. Two additional Case objects (459 and 460) are emission regions within the same galaxy, and we choose to count them as one object for the purpose of the comparison with KISS. Of the resulting 15 Case objects, 13 (87%) are recovered by KISS in the main survey (i.e., Table 2). This fraction of recovered objects is somewhat higher than what was found for the first two red surveys (73% and 72% respectively). Both of the two Case galaxies that KISS does not recover are listed as color-selected in the Case survey papers. Neither one is listed in the secondary KISS survey list with  $4\sigma$  to  $5\sigma$  ELG candidates. A large fraction of Case galaxies have  $H\alpha$  lines with equivalent widths less than  $30 \text{ \AA}$  (Salzer *et al.* 1995), and KISS is not as sensitive to this type of object.

The UGC catalog overlaps with the Boötes field, and there are eight UGC galaxies in this area. Four of them are also KISS galaxies. Weak emission lines appear to be

present in the objective-prism spectra of the remaining four galaxies, but only at the  $\sim 3\sigma$  level.

#### 5. DISCUSSION & SUMMARY

We present the third list of  $H\alpha$ -selected emission-line galaxy candidates (and fourth list overall) from the KPNO International Spectroscopic Survey (KISS). All data presented here were obtained with the 0.61-m Burrell Schmidt telescope. KISS is an objective-prism survey, but differs from older such surveys by virtue of the fact that it utilizes a CCD as the detector. While we sacrifice areal coverage relative to classical photographic surveys, we benefit from the enormous gain in sensitivity that CCDs provide over plates. We readily detect strong-lined ELGs as faint as  $B = 21$ . In addition, the pan-chromatic nature of CCDs allows us greater wavelength agility compared to photographic surveys. Even with the use of our survey filter, which restricts the detection of ELGs to  $z < 0.095$ , we are sensitive to a broader range of galaxian redshifts than the older photographic objective-prism surveys (Paper I). The combination of higher sensitivity, lower noise, and larger volumes surveyed yield huge improvements in the depth of the resulting survey. With the KISSRx objects included, KISS finds  $>200$  times more AGN and starburst galaxy candidates per unit area than did the Markarian (1967) survey, and  $\sim 37$  times more than the UCM survey (Zamorano *et al.* 1994).

The current installment of KISS includes 261 ELG candidates selected from 20 red survey fields covering a total of  $19.65 \text{ deg}^2$ . This yields a surface density of  $13.3$  galaxies per  $\text{deg}^2$ . We are sensitive to the  $H\alpha$  emission line with redshifts up to  $\sim 0.10$ . The survey fields presented here are located at  $RA = 14^h 30^m$ ,  $\delta = 34^\circ 30'$  (B1950), and at  $RA = 2^h 7.5^m$ ,  $\delta = -4^\circ 44'$ . These fields were chosen to coincide with the location of the NOAO Deep Wide-Field Survey (Jannuzi & Dey 1999). For each object in the catalog we tabulate accurate equatorial coordinates, B & V photometry, and estimates of the redshift and line strength measured from the objective-prism spectra. We also provide finder charts and extracted spectral plots for all objects. In addition to the main survey list, we include a supplementary list of 158 ELG candidates with weaker (lower significance) emission lines.

This newest list brings the total of  $H\alpha$ -selected KISSR ELGs to 2418 objects present in three survey regions. In addition, we have cataloged another 638 “extra” KISSRx candidates that are detected in the survey with a lower significance level. The total number of cataloged ELGs is 3056, contained in a survey area of just  $147.6 \text{ sq. deg.}$ . The overall surface density of KISS ELGs is thus  $20.7$  per sq. deg.

One of the advantages of our survey method is the large amount of basic data that we acquire for each object. This in turn allows us to parameterize the constituents of the survey and to develop a fairly complete picture of the overall sample without the need for extensive follow-up observations. We present an overview of the survey properties for the current list of ELG candidates. The median apparent magnitude of the current sample is  $B = 17.91$ . This is somewhat brighter than the values found for KR1 and KR2 ( $B = 18.08$  and  $18.13$ , respectively), but it is still substantially fainter than pre-

vious ELG surveys. Objects fainter than  $B = 20$  are routinely cataloged. Line strengths measured from the objective-prism spectra show that KISS is sensitive to objects with  $H\alpha + [N II]$  equivalent widths of less than 20 Å, and that most objects with  $EW > 40$  Å are detected. The median emission-line flux of the KISS sample is nearly three times lower than that of the UCM survey (Gallego *et al.* 1996). The luminosity distribution of the KISS ELGs is heavily weighted toward intermediate- and low-luminosity galaxies, although we are still sensitive to luminous AGN and starbursting galaxies. The median absolute magnitude of  $M_B = -19.11$  underscores the fact that strong-lined galaxies of the type cataloged by KISS tend to be less luminous than the types of objects found in more traditional magnitude-limited samples.

Despite the fact that one can learn a great deal about each KISS ELG from the survey data alone, it is still necessary to obtain higher dispersion follow-up spectra in order to arrive at a more complete understanding of each object. For example, due to the low-dispersion nature of the objective-prism spectra it is not possible to distinguish between AGN and star-formation activity in the KISS galaxies. Further, the redshifts derived from the KISS spectral data are too coarse to be used in detailed spatial distribution studies. We have obtained follow-up spectra for 100% of KISS ELGs in the KR1 and KB1 survey lists, and we are in the process of obtaining spectra for the objects in the remaining survey lists (KR2 and the current list. These follow-up spectra will allow

us to better assess the nature of the individual galaxies, which in turn enables the sample to be used for a wide variety of science applications, many of which are outlined in Paper I. Examples include a series of multi-wavelength studies of the properties of KISS ELGs in the radio (Van Duyne *et al.* 2004) and X-rays (Stevenson *et al.* 2002, Datta *et al.* 2006, in preparation), plus studies currently underway in the mid- and far-IR (IRAS and Spitzer) and near-IR (2MASS), as well as ongoing studies of the metal abundances in KISS star-forming galaxies (e.g., Lee *et al.* 2004, Salzer *et al.* 2005).

We gratefully acknowledge financial support for the KISS project through NSF Presidential Faculty Award to JJS (NSF-AST-9553020), which was instrumental in initiating the original international collaboration, as well as continued support via NSF-AST-0071114 and NSF-AST-0307766. CG also acknowledges support from NSF-AST-0137927. We thank the numerous colleagues with whom we have discussed the KISS project over the past several years, including Jesús Gallego, Rafael Guzmán, Rob Kennicutt, David Koo, Trinh Thuan, Alexei Kniazev, Yuri Izotov, Janice Lee, Jason Melbourne and Jose Herero. Finally, we wish to thank the Astronomy Department of Case Western Reserve University for maintaining the Burrell Schmidt during the period of time when the survey observations reported here were obtained.

## APPENDIX

### SUPPLEMENTARY TABLE OF $4\sigma$ OBJECTS

As we explained in Section 3, the main survey objects are selected based on the presence of a  $5\sigma$  emission feature in their spectra. Because of the high sensitivity of the survey data, many objects were detected that have apparent emission lines with strengths that are only slightly weaker than the  $5\sigma$  limit. We decided to exclude such objects from the main survey list since one of the primary goals of the KISS project is to construct a deep but statistically complete sample of ELGs. Early tests involving follow-up spectroscopy carried out on fields where objects were selected to lower thresholds showed that  $5\sigma$  detections were nearly always real sources, while objects between  $4\sigma$  and  $5\sigma$  tended to be real but also included a fair number ( $\sim 25\%$ ) of spurious sources. However, these objects are nonetheless valid ELG candidates, and this list of objects likely includes a number of interesting objects. Therefore, rather than ignore these weaker-lined ELG candidates entirely, we are publishing them in a supplementary table.

Listed in Table 4 are 158 ELG candidates that have emission lines detected at between the  $4\sigma$  and  $5\sigma$  level. The format of Table 4 is the same as for Table 2, except that the objects are now labeled with KISSRx numbers ('x' for extra). The KISSRx numbers start at 481 since we presented 480 KISSRx objects in KR1 and KR2. The full version of the table, as well as finder charts for all 158 KISSRx galaxies, are available in the electronic version of the paper.

The supplementary ELG sample has characteristics similar to those of the main survey ELGs, although with some notable differences. The median  $H\alpha$  equivalent width is 40.9 Å, roughly 20% lower than the value for the main sample. The KISSRx galaxies are somewhat fainter (median  $B$  magnitude of 18.65) and significantly redder (median  $B-V = 0.81$ ). Their median redshift is slightly higher than that of either the Boötes or Cetus field (0.067), and their median luminosity is nearly a magnitude fainter ( $-18.23$ ). Hence, the supplementary ELG list appears to be dominated by intermediate luminosity galaxies with somewhat lower rates of star-formation activity (lower equivalent widths, redder colors) than the ELGs in the main sample. The differences between the KISSR and KISSRx objects in the current paper are similar to those seen between the two samples in KR1 and KR2.

## REFERENCES

- Falco, E. E., Kurtz, M. J., Geller, M. J., Huchra, J. P., Peters, J., Berlind, P., Mink, D. J., Tokarz, S. P., & Elwell, B. 1999, *PASP*, 111, 438
- Gallego, J., Zamorano, J., Rego, M., Alonso, O., & Vitores, A. G. 1996, *A&AS*, 120, 323
- Gronwall, C., Salzer, J. J., Sarajedini, V. L., Jangren, A., Chomiuk, L. B., Moody, J. W., Frattare, L. M., & Boroson, T. A. 2004, *AJ*, 127, 1943 (KR2)
- Gronwall, C., Salzer, J. J., Brenneman, L., Condy, E., & Santos, M. 2005, in preparation
- Huchra, J. P., & Sargent, W. L. W. 1973, *ApJ*, 186, 433
- Jannuzi, B. T., & Dey, A., 1999, in *Photometric Redshifts and the Detection of High Redshift Galaxies*, ASP Conference Series, Vol. 191, ed. R. Weymann, L. Storrie-Lombardi, M. Sawicki, and R. Brunner, p. 111
- Kirshner, R. P., Oemler, A., Jr., Schechter, P. L., & Shectman, S. A. 1981, *ApJ*, 248, L57
- Lee, J. C., Salzer, J. J., & Melbourne, J. 2004, *ApJ*, 616, 752
- MacAlpine, G. M., Smith, S. B., & Lewis, D. W. 1977, *ApJS*, 34, 95
- Markarian, B. E. 1967, *Astrofizika*, 3, 55
- Markarian, B. E., Lipovetskii, V. A., & Stepanian, D. A. 1983, *Astrofizika*, 19, 29
- Mazzarella, J. M., & Balzano, V. A. 1986, *ApJS*, 62, 751
- Nilson, P. 1973, *Uppsala General Catalogue of Galaxies*, (Uppsala: Roy. Soc. Sci. Uppsala)
- Pérez-González, P. G., Zamorano, J., Gallego, J., & Gil de Pez, A. 2000, *A&AS*, 141, 409
- Pesch, P., & Sanduleak, N. 1983, *ApJS*, 51, 171
- Popescu, C. C., Hopp, U., Hagen, H. J., & Elsässer, H. 1996, *A&AS*, 116, 43
- Roberts, M. S., & Haynes, M. P. 1994, *ARA&A*, 32, 115
- Salzer, J. J., Gronwall, C., Lipovetsky, V. A., Kniazev, A., Moody, J. W., Boroson, T. A., Thuan, T. X., Izotov, Y. I., Herrero, J. L., & Frattare, L. M. 2000, *AJ*, 120, 80 (Paper I)
- Salzer, J. J., Gronwall, C., Lipovetsky, V. A., Kniazev, A., Moody, J. W., Boroson, T. A., Thuan, T. X., Izotov, Y. I., Herrero, J. L., & Frattare, L. M. 2001, *AJ*, 121, 66 (KR1)
- Salzer, J. J., Gronwall, C., Sarajedini, V. L., Lipovetsky, V. A., Kniazev, A., Moody, J. W., Boroson, T. A., Thuan, T. X., Izotov, Y. I., Herrero, J. L., & Frattare, L. M. 2002, *AJ*, 123, 1292 (KB1)
- Salzer, J. J., Lee, J. C., Melbourne, J., Hinz, J., Alonso-Herrero, A., & Jangren, A. 2005, *ApJ*, 624, 661
- Salzer, J. J., MacAlpine, G. M., & Boroson, T. A. 1989, *ApJS*, 70, 479
- Salzer, J. J., Moody, J. W., Rosenberg, J. L., Gregory, S. A., & Newberry, M. V. 1995, *AJ*, 109, 2376
- Schlegel, D. J., Finkbeiner, D. P., & Davis, M. 1998, *ApJ*, 500, 525
- Schmidt, M. 1968, *ApJ*, 151, 393
- Smith, M. G., Aguirre, C., & Zemelman, M. 1976, *ApJS*, 32, 217
- Stevenson, S. L., Salzer, J. J., Sarajedini, V. L., & Moran, E. C. 2002, *AJ*, 124, 3465
- Surace, C., & Comte, G. 1998, *A&AS*, 133, 171
- Ugryumov, A. V., *et al.* 1999, *A&AS*, 135, 511
- Van Duyne, J., Beckerman, E., Salzer, J. J., Gronwall, C., Thuan, T. X., Condon, J. J., & Frattare, L. M. 2004, *AJ*, 127, 1959
- Wasilewski, A. J. 1983, *ApJ*, 272, 68
- Zamorano, J., Rego, M., Gallego, J., Vitores, A. G., González-Riestra, R., & Rodríguez-Caderot, G. 1994, *ApJS*, 95, 387
- Zwicky, F., Herzog, E., Kowal, C. T., Wild, P., & Karpowicz, M. 1961–1968, *Catalogue of Galaxies and Clusters of Galaxies*, (Pasadena: CIT) (CGCG)

TABLE 1  
KISS NDWF RED SURVEY OBSERVING RUNS

Dates of Run (1)	Number of Nights <sup>a</sup> (2)	Number of Fields – Direct <sup>b</sup> (3)	Number of Fields – Spectral <sup>b</sup> (4)
June 23 – 24, 1998	2	8	...
September 17 – 19, 1998	3	...	10
November 19 – 23, 1998	3	12	...
May 12 – 14, 1999	3	...	8
November 6, 1999	1	...	2

<sup>a</sup>Number of nights during run that data were obtained.

<sup>b</sup>Number of survey fields observed.

TABLE 2  
LIST OF CANDIDATE ELGS

KISSR # (1)	Field (2)	ID (3)	R.A. (J2000) (4)	Dec. (J2000) (5)	B (6)	B–V (7)	$z_{KISS}$ (8)	Flux <sup>a</sup> (9)	EW [Å] (10)	Qual. (11)	Comments (12)
2158	H0202	4755	2 01 59.3	-4 41 03.5	17.88	0.59	0.0286	53	26	2	
2159	G0202	3879	2 02 18.2	-3 42 09.9	18.97	1.37	0.0871	34	21	3	
2160	G0202	3858	2 02 18.8	-3 36 50.7	18.43	0.50	0.0415	72	64	1	
2161	G0202	3653	2 02 26.0	-4 11 05.9	15.25	0.47	0.0159	353	50	1	
2162	G0202	3213	2 02 39.4	-4 09 01.7	15.91	0.59	0.0465	316	28	2	
2163	G0202	3037	2 02 44.0	-3 52 35.2	18.49	0.38	0.0143	46	36	2	
2164	G0202	3055	2 02 44.1	-4 11 17.8	19.05	0.51	0.0430	39	60	2	
2165	G0202	2729	2 02 53.9	-4 07 19.7	16.45	0.84	0.0435	138	14	1	
2166	G0202	2315	2 03 05.8	-3 50 24.8	16.57	0.90	0.0427	38	4	3	
2167	G0202	2317	2 03 06.4	-4 15 05.9	19.48	0.92	0.0811	39	47	2	
2168	G0202	2329	2 03 06.5	-4 27 14.1	17.11	0.41	0.0155	245	72	1	
2169	G0202	2135	2 03 13.2	-4 18 47.3	19.01	0.83	0.0909	50	94	3	
2170	G0202	1836	2 03 21.4	-4 03 31.0	18.05	0.87	0.0650	81	33	1	
2171	H0202	2122	2 03 25.5	-5 04 24.4	20.01	0.51	0.0547	69	3054	3	
2172	G0202	1224	2 03 42.3	-4 45 18.3	17.19	0.81	0.0370	54	9	3	
2173	G0202	1148	2 03 42.9	-3 49 15.4	16.78	0.71	0.0469	410	57	1	
2174	G0202	786	2 03 54.0	-3 53 00.1	15.76	0.63	0.0425	863	65	1	
2175	G0202	646	2 03 58.9	-4 01 15.2	17.96	0.96	0.0617	68	24	1	
2176	G0202	550	2 04 00.9	-3 16 08.8	21.00	1.68	0.0902	33	342	3	
2177	H0202	807	2 04 08.2	-4 50 47.1	17.78	0.53	0.0771	117	97	1	
2178	G0202	420	2 04 08.5	-4 49 15.4	18.13	1.17	0.0829	45	25	2	
2179	G0202	372	2 04 09.5	-4 28 20.2	18.33	0.79	0.0793	89	54	1	
2180	H0202	549	2 04 16.9	-4 48 41.0	17.29	0.70	0.0869	77	24	1	
2181	G0202	76	2 04 17.0	-3 39 15.2	19.17	0.90	0.0777	66	101	2	
2182	H0202	434	2 04 20.3	-4 54 58.1	14.99	0.28	0.0178	151	32	1	
2183	G0205	5741	2 04 21.7	-3 42 40.0	17.71	0.83	0.0586	54	22	1	
2184	G0205	5425	2 04 30.4	-3 36 09.1	17.71	0.76	0.0558	72	23	1	
2185	G0205	5416	2 04 31.4	-4 03 34.6	19.56	0.67	0.0387	59	168	1	
2186	G0205	5375	2 04 33.4	-4 29 39.6	17.83	0.45	0.0483	97	65	1	
2187	H0205	6171	2 04 35.9	-5 30 00.0	18.12	0.78	0.0764	151	92	1	

Note. – The complete version of this table is presented in the electronic edition of the Journal. A portion is shown here for guidance regarding its content and format.

<sup>a</sup>Units of  $10^{-16}$  erg/s/cm<sup>2</sup>

TABLE 3  
 $V/V_{max}$  TEST

$m_L$	Total Number	Number Flux Limited	Number Volume Limited	$\langle V/V_{max} \rangle$	Number added	Cumulative number added	% Flux Limited	% Complete
(1)	(2)	(3)	(4)	(5)	(6)	(7)	(8)	(9)
13.0	4	4	0	0.5922	0	0	100.00	100.00
13.1	5	5	0	0.5900	0	0	100.00	100.00
13.2	5	5	0	0.5139	0	0	100.00	100.00
13.3	7	7	0	0.5889	0	0	100.00	100.00
13.4	8	8	0	0.5688	0	0	100.00	100.00
13.5	9	9	0	0.5468	0	0	100.00	100.00
13.6	12	12	0	0.5928	0	0	100.00	100.00
13.7	16	16	0	0.6271	0	0	100.00	100.00
13.8	20	20	0	0.6256	0	0	100.00	100.00
13.9	22	20	2	0.5666	0	0	90.91	100.00
14.0	28	24	4	0.6046	0	0	85.71	100.00
14.1	35	28	7	0.6352	0	0	80.00	100.00
14.2	38	31	7	0.5891	0	0	81.58	100.00
14.3	44	36	8	0.5833	0	0	81.82	100.00
14.4	54	42	12	0.5818	0	0	77.78	100.00
14.5	67	50	17	0.5946	0	0	74.63	100.00
14.6	81	56	25	0.6012	0	0	69.14	100.00
14.7	98	67	31	0.6173	0	0	68.37	100.00
14.8	108	69	39	0.5764	0	0	63.89	100.00
14.9	120	76	44	0.5646	0	0	63.33	100.00
15.0	139	87	52	0.5642	0	0	62.59	100.00
15.1	154	93	61	0.5480	0	0	60.39	100.00
15.2	166	99	67	0.5251	0	0	59.64	100.00
15.3	184	106	78	0.5122	0	0	57.61	100.00
15.4	195	107	88	0.4822	4	4	54.87	96.40
15.5	206	114	92	0.4612	6	10	55.34	91.94
15.6	216	117	99	0.4330	9	19	54.17	86.03
15.7	225	120	105	0.4104	10	29	53.33	80.54
15.8	231	119	112	0.3821	13	42	51.52	73.91
15.9	238	117	121	0.3761	10	52	49.16	69.23
16.0	244	110	134	0.3417	17	69	45.08	61.45
16.1	253	104	149	0.3333	13	82	41.11	55.91
16.2	257	94	163	0.3116	16	98	36.58	48.96
16.3	259	88	171	0.2757	21	119	33.98	42.51
16.4	260	83	177	0.2521	22	141	31.92	37.05
16.5	261	76	185	0.2258	24	165	29.12	31.54

TABLE 4  
LIST OF  $4\sigma$  CANDIDATE ELGS

KISSRx # (1)	Field (2)	ID (3)	R.A. (J2000) (4)	Dec. (J2000) (5)	B (6)	B-V (7)	$z_{KISS}$ (8)	Flux <sup>a</sup> (9)	EW [Å] (10)	Qual. (11)	Comments (12)
481	G0202	5949	2 01 17.5	-3 54 59.0	18.12	0.57	0.0396	43	19	2	
482	G0202	5213	2 01 41.7	-4 16 42.6	21.07	1.88	0.0816	79	116	3	
483	G0202	4890	2 01 49.8	-3 46 50.7	18.98	0.77	0.0729	92	71	2	
484	G0202	4563	2 01 57.6	-3 17 19.8	19.27	0.76	0.0407	29	43	3	
485	G0202	4294	2 02 07.1	-4 05 04.2	19.13	1.05	0.0597	59	32	2	
486	G0202	4158	2 02 11.2	-4 07 33.9	17.76	1.03	0.0849	50	19	3	
487	G0202	2393	2 03 04.4	-4 28 15.8	17.89	1.03	0.0370	51	18	2	
488	G0202	2057	2 03 13.9	-3 19 42.6	20.58	0.57	0.0767	49	228	3	
489	G0202	1608	2 03 27.2	-3 17 14.9	17.74	0.15	0.0375	46	32	2	
490	G0202	1499	2 03 31.6	-3 46 56.4	19.07	0.70	0.0873	39	33	3	
491	H0202	1892	2 03 32.0	-4 21 50.5	20.42	1.16	0.0515	64	105	2	
492	H0202	1443	2 03 46.9	-4 35 15.3	19.10	0.82	0.0546	43	6	3	
493	H0202	749	2 04 09.5	-4 28 19.8	18.34	0.75	0.0733	121	69	2	
494	G0205	4694	2 04 53.7	-4 00 57.6	19.44	0.24	0.0135	31	111	3	
495	G0205	4052	2 05 12.1	-3 28 55.0	19.35	0.74	0.0674	93	50	2	
496	G0205	3412	2 05 33.2	-3 57 25.3	18.78	0.65	0.0926	44	54	2	
497	G0205	3002	2 05 45.8	-3 15 37.4	23.42	3.92	0.0713	67	84	3	
498	G0205	2790	2 05 52.7	-3 23 46.0	18.30	0.82	0.0827	20	11	3	
499	H0205	3297	2 06 00.2	-4 40 31.8	23.69	3.69	0.0673	40	322	3	
500	H0205	3071	2 06 08.5	-5 20 22.8	19.37	0.73	0.0744	32	35	2	
501	G0205	2173	2 06 14.5	-4 28 14.9	18.16	0.13	0.0341	53	45	2	
502	G0205	1969	2 06 21.7	-4 13 34.2	16.73	0.67	0.0346	75	11	2	
503	G0205	1809	2 06 25.4	-3 29 24.8	21.11	1.16	0.0684	28	57	2	
504	G0205	1512	2 06 35.9	-3 38 17.3	16.35	0.27	0.0284	115	12	3	
505	G0205	1496	2 06 37.6	-4 19 43.9	19.82	1.48	0.0388	30	19	3	
506	H0205	1656	2 06 50.8	-5 32 50.7	18.52	0.84	0.0245	32	19	3	
507	G0205	943	2 06 54.0	-3 35 21.2	19.68	1.20	0.0682	40	28	2	
508	H0205	1333	2 07 01.1	-5 47 59.0	18.66	0.66	0.0345	44	32	3	
509	G0205	417	2 07 10.9	-3 30 36.5	19.50	0.89	0.0763	84	362	2	
510	G0205	52	2 07 21.7	-3 15 56.5	19.89	0.81	0.0091	52	64	3	

Note.— The complete version of this table is presented in the electronic edition of the Journal. A portion is shown here for guidance regarding its content and format.

<sup>a</sup>Units of  $10^{-16}$  erg/s/cm<sup>2</sup>